Geomechanics and Engineering, *Vol. 11, No. 2 (2016) 211-234*
DOI: http://dx.doi.org/10.12989/gae.2016.11.2.211

Characterization and uncertainty of uplift load-displacement behaviour of belled piers

Xian-long Lu [1a], Zeng-zhen Qian [*2], Wei-feng Zheng [1b] and Wen-zhi Yang [1c]

[1] *China Electric Power Research Institute, No. 15, Xiaoying East Road, Haidian District, Beijing, 100192, China*
[2] *School of Engineering and Technology, China University of Geosciences, No. 29 Xueyuan Road, Haidian District, Beijing, 100083, China*

(*Received February 12, 2015, Revised February 11, 2016, Accepted April 27, 2016*)

Abstract. A total of 99 full-scale field load tests at 22 sites were compiled for this study to elucidate several issues related to the load-displacement behaviour of belled piers under axial uplift loading, including (1) interpretation criteria to define various elastic, inelastic, and "failure" states for each load test from the load-displacement curve; (2) generalized correlations among these states and determinations to the predicted ultimate uplift resistances; (3) uncertainty in the resistance model factor statistics required for reliability-based ultimate limit state (ULS) design; (4) uncertainty associated with the normalized load-displacement curves and the resulting model factor statistics required for reliability-based serviceability limit state (SLS) design; and (5) variations of the combined ULS and SLS model factor statistics for reliability-based limit state designs. The approaches discussed in this study are practical and grounded realistically on the load tests of belled piers with minimal assumptions. The results on the characterization and uncertainty of uplift load–displacement behaviour of belled piers could be served as to extend the early contributions for reliability-based ULS and SLS designs.

Keywords: belled piers; uplift; load tests; reliability-based design; model uncertainty; normalized load-displacement curve; hyperbolic curve-fitting parameters

1. Introduction

Belled piers have been widely used to satisfy the uplift resistance requirements for transmission tower structures in China. In the design of belled piers under an axial uplift loading, the overall load–displacement behaviour plays an important role, first in estimating displacement at a given load and second in interpreting the failure load or uplift resistance. Therefore, it is essential to characterize their uplift load–displacement behaviours and their uplift resistance evaluations.

A number of different failure interpretation criteria based on a variety of assumptions have been recommended in geotechnical literatures (e.g., Terzaghi and Peck 1967, Chin 1970, DeBeer 1970, Fuller and Hoy 1970, Davisson 1972, O'Rourke and Kulhawy 1985, Hirany and Kulhawy 1988,

*Corresponding author, Ph.D., E-mail: zzqian@cugb.edu.cn
[a] Ph.D., E-mail: luxianlong@163.com
[b] Ph.D., E-mail: zhengweifeng1977@126.com
[c] M.Sc., Civil Engineer, E-mail: yangwenzhi@epri.sgcc.com.cn

 ISSN: 2005-307X (Print), 2092-6219 (Online)

1989, 2002). The procedures for assessing different load tests have been verified for drilled shafts (Chen 2004, Chen *et al*. 2008, 2011, Chen and Lee 2010, Chen and Chu 2012, Qian *et al*. 2014a), augered cast-in-place piles (Chen 1998, Ching and Chen 2010), pressure-injected footings (Chen 1998, Chen and Kulhawy 2002, 2003), driven piles (Marcos *et al*. 2013), and micropiles (Kulhawy and Jeon 1999, Jeon and Kulhawy 2001). Therefore, it is worthwhile to examine these criteria over belled piers and to characterize their uplift load–displacement behaviours.

In limit state designs, it is important to consider the ultimate limit state (ULS) (dealing with foundation resistance) and the serviceability limit state (SLS) (dealing with foundation displacement) simultaneously. Therefore, the majority of research on belled piers should be devoted both to the ultimate load resistance and to the estimation of displacement at the service load level.

For the ULS, the resistance model factor is typically defined as the ratio of the measured resistance to the predicted or calculated resistance. However, it is a fact that the predicted resistance is performed under a considerable degree of uncertainty. Research studies have indicated that model uncertainty is an important factor (Phoon and Kulhawy 2008, Dithinde *et al*. 2011). Model uncertainty arises from unavoidable idealizations and simplifications in the analytical model for predicting geotechnical behaviours even if the model inputs are known with certainty. The ultimate uplift resistances for belled piers are determined on the basis of a theoretical model, but the lack of resistance model statistics may be a key impediment to the development of geotechnical reliability-based design (Phoon 2005). As a result, there is a need for the effort to develop resistance model factor statistics for belled piers.

For the SLS, it is convenient to capture the uncertainties in the nonlinear load–displacement curves using two hyperbolic curve-fitting parameters (Phoon *et al*. 2007). Chin (1970, 1978) used it to characterize load–displacement curves obtained from static pile loading tests. Stewart and Kulhawy (1990) used this approach to characterize uplift load–displacement curves obtained from full-scale tests of grillage foundations. To develop statistics for the uncertainties in nonlinear load–displacement curves, the uncertainty in the load–displacement behaviour can be characterized by fitting the measured load–displacement data to a hyperbolic equation and by normalizing the hyperbolic curve with the interpreted resistance (Phoon and Kulhawy 2008, Dithinde *et al*. 2011, Akbas and Kulhawy 2009).

With the increasing implementation of reliability-based design (RBD) in engineering practice, there is greater emphasis on characterizing design uncertainty and quantifying the probability of exceeding a particular limit state (Phoon 2008, Phoon and Kulhawy 2008, Li *et al*. 2013, Chen *et al*. 2014, Huffman and Stuedlein 2014). To meet the requirements for the ULS and SLS designs, there is a need to develop procedures that can accurately and reliably predict the uplift resistance and displacement of belled piers with regard to the multiple sources of uncertainty that contribute to the prediction variability.

In this study, an extensive database of 99 load tests at 22 sites conducted in China was compiled to characterize the overall axial uplift load–displacement behaviour of belled piers. The load test data were interpreted using six representative interpretation criteria to define various elastic, inelastic, and "failure" states for each load test. These results were interrelated to establish generalized correlations among these states and to determine the predicted ultimate uplift resistances. The resistance model factor was defined as the ratio of the interpreted uplift resistance (L_1–L_2 method) and the predicted resistance [determined by the Meyerhof and Adams (1968) design formula]. The resistance model factor statistics were obtained for reliability-based ULS design in this study. The uncertainty in the load–displacement behaviour was characterized by

normalizing the measured load–displacement data with predicted ultimate uplift resistances and then by fitting each of the normalized load–displacement curves with a hyperbolic equation. The hyperbolic curve-fitting parameter statistics were obtained for reliability-based SLS design, and they were presented by different confidence limit levels. The resulting curves were suggested to indicate the normalized loads versus the corresponding displacements at the confidence limit levels of the mean, plus and minus one standard deviation (SD), and 95% confidence limit level. Finally, the variations of the combined ULS and SLS model factor statistics were presented for reliability-based limit state designs.

2. Load test database

The database developed for this study included 99 axial uplift field load tests on belled piers conducted at 22 sites in Chinese overhead transmission line engineering. Appendix A shows the location of each load test site and the general description of the soil.

Fig. 1 shows the general form and the geometric symbols of a belled pier, where D is the depth from the ground surface to the bottom of foundation slab, b is the shaft diameter, B is the bell diameter, t is the bedding cushion thickness, e is the height above the ground surface, and θ is the angle which the pyramidal or conical surface makes against the vertical.

In Chinese transmission line engineering, belled piers are usually excavated by labour forces. This dry method of manually excavating the shafts is commonly employed in the soil that is above the water table and that will not cave or slump when the hole is excavated to its full dimension during the period required for the installation of the foundation. All the belled piers in this study were constructed without water encountering. Appendix B shows dimensions of the belled piers and the prevailing soil properties.

The construction for a belled shaft is performed by two steps. The first step is to excavate the shaft to the required depth and diameter, and the second step is to enlarge the circular base to the required dimensions. During excavating, the diameter and the verticality of each shaft are measured at an interval of approximately 1 m until the required depth is achieved. All of the dimensional values in Appendix B are the means of the measured data, and all of the foundation shafts had truly vertical faces.

Each of the load tests was conducted after the concrete had cured for approximately 28 days. All of the tests were conducted with static monotonic loading and without cycling.

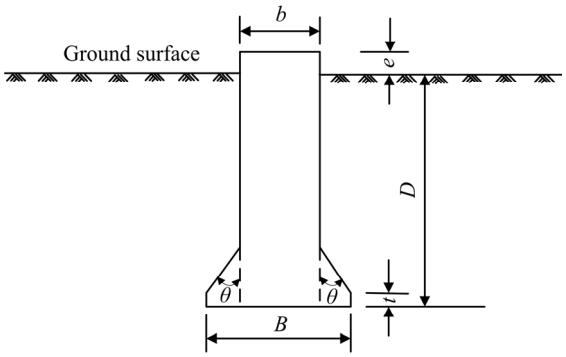

Fig. 1 General form and geometrical symbols of a belled pier

3. Determination of interpreted and predicted capacities

3.1 Interpreted loads and displacements

Fig. 2 shows four typical axial uplift load–displacement curves for belled piers. These curves differs in the ratio of the applied load to the uplift resistance, but all approximately exhibits an initial linear, a curvilinear transition, and a final linear region as illustrated in Fig. 3. In general, the load–displacement curves obtained from the uplift loads test did not provide a well-defined peak or asymptotic value of the load; therefore, estimating the uplift failure load needed to be interpreted as done in the previous studies (Akbas and Kulhawy 2009, Briaud 2007, Chen 2004, Chen *et al*. 2008, Chen and Chu 2012, Chen and Fang 2009, Marcos *et al*. 2013, Qian *et al*. 2014a).

In this study, six different interpretation criteria listed in Table 1 were used to evaluate the uplift interpreted failure resistance from the load–displacement curve of each belled pier. These criteria were selected because they represent a distribution of interpreted results from the lower, middle, and higher ranges as found in practices (Chen 2004, Chen *et al*. 2008, Chen and Chu 2012, Chen and Fang 2009, Marcos *et al*. 2013, Qian *et al*. 2014a). In addition, these criteria employ varied interpretation bases, as noted in Table 1. Therefore, they can be considered as representative of existing criteria.

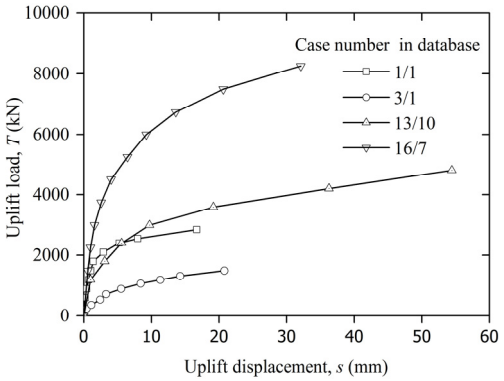

Fig. 2 Typical axial uplift load–displacement curves for belled piers

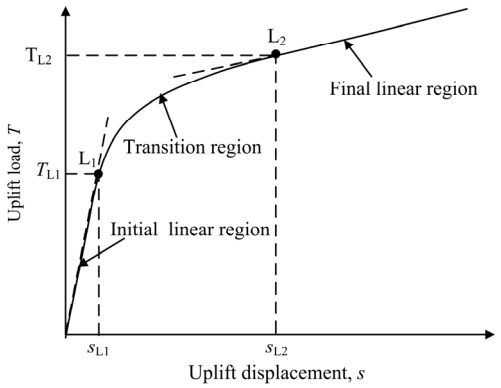

Fig. 3 Regions of load–displacement curve for the L_1–L_2 method (Hirany and Kulhawy 1988, 1989, 2002)

Table 1 Definitions of representative uplift interpretation criteria

Method	Category	Definition of interpreted failure resistance, T
Chin (1970)	Mathematical modeling	T_{CHIN} is equal to the inverse slope, 1/m, of the line, $s/T = ms + c$, where T is the uplift load; s is the total displacement; and m, c is the slope and intercept of the line, respectively.
Terzaghi and Peck (1967)	Displacement limitation	$T_{T\&P}$ is the load that occurs at 1.0 in. (25.4 mm) total displacement.
Davisson (1972)	Displacement limitation	T_{DA} occurs at a displacement equal to the shaft elastic uplift line, PD/EA, offset by 0.15 in. (3.8 mm), where P = uplift load; D = depth; A = area; and E = Young's modulus.
Slope tangent (O'Rourke and Kulhawy 1985)	Graphical construction	T_{ST} occurs at a displacement equal to the initial slope of the load–displacement curve plus 0.15 in. (3.8 mm).
Tangent Intersection (Housel 1966, Tomlinson 1977)	Graphical construction	T_{TI} is determined as the intersection of two lines drawn as tangents to the initial linear and final linear portions of the load–displacement curve and projected to the load–displacement curve.
L_1–L_2 (Hirany and Kulhawy 1988, 1989, 2002)	Graphical construction	T_{L1} and T_{L2} correspond to elastic limit and failure threshold loads, respectively, as shown in Fig. 3.

The definition of interpreted failure load or resistance by Chin (1970) is based on a mathematical model that corresponds to the asymptote of the load–displacement curve. The interpreted capacities by Terzaghi and Peck (1967) is defined as the load at an absolute total displacement of 1.0 in. (25.4 mm). The Davisson method (1972) is a graphical construction and defines the resistance at the intersection of the load–displacement curve and the shaft elastic uplift line offset by 3.8 mm. The slope tangent method (O'Rourke and Kulhawy 1985) is a modification of the Davisson method (Davisson 1972) and uses the initial slope instead of the elastic line. The failure load is determined from the intersection of a line drawn parallel to the initial linear portion of the load–displacement curve at a distance equivalent to a displacement of 3.8 mm. The tangent intersection method (Housel 1966, Tomlinson 1977) has also been used to interpret the failure load, which is determined as the intersection of two lines drawn as tangents to the initial linear and final linear portions of the load–displacement curve. The L_1–L_2 method (Hirany and Kulhawy 1988, 1989, 2002) is based on the fact that a load–displacement curve can generally be simplified into three distinct sectors: initial linear, non-linear curve transition, and final linear, as illustrated in Fig. 3. Point L_1 (elastic limit) corresponds to the load (T_{L1}) and displacement (s_{L1}) at the end of the initial linear region, whereas L_2 (failure threshold) corresponds to the load (T_{L2}) and displacement (s_{L2}) at the beginning of the final linear region.

The interpreted uplift resistances T_{L1}, T_{DA}, T_{ST}, T_{TI}, $T_{T\&P}$, T_{L2}, and T_{CHIN}, as well as the corresponding displacements s_{L1}, s_{DA}, s_{ST}, s_{TI}, s_{L2}, and s_{CHIN} for all the tests are shown in Appendix C. It should be noted that T_{L1} was included for reference only, and it is not an interpreted failure load or resistance, but the elastic limit.

Table 2 Summary of statistics for interpreted loads and displacements

Statistics	Ratios among interpreted loads, T/T_{L2}						Displacement at interpreted criteria, s[a] (mm)					
	T_{L1}	T_{DA}	T_{ST}	T_{TI}	$T_{T\&P}$	T_{CHIN}	s_{L1}	s_{DA}	s_{ST}	s_{TI}	s_{L2}	s_{CHIN}
Minmun	0.28	0.34	0.50	0.47	0.79	1.03	0.01	3.78	2.54	0.97	2.50	> 4.42[b]
Mean	0.46	0.73	0.84	0.92	1.03	1.20	1.52	4.14	6.39	10.24	15.72	> 41.11
Maximum	0.88	1.03	1.03	1.02	1.27	1.58	6.10	5.28	15.59	25.80	52.20	> 96.57
SD	0.13	0.14	0.13	0.09	0.06	0.12	1.22	0.31	2.15	4.85	9.38	20.36
COV	0.28	0.20	0.15	0.09	0.06	0.10	0.80	0.07	0.34	0.47	0.60	0.50

[a] by definition, $s_{T\&P}$ = 25.4 mm, and there is no statistics.
[b] The symbol (>) expresses that the interpreted displacements are greater than the measured data

3.2 Evaluation of load test results and determinaton of measured uplift resistances

All of the interpreted uplift resistances were normalized by the failure threshold, T_{L2}, of L_1–L_2 method. The L_1–L_2 method could interpret all the load test cases in this study, and T_{L2} is generally defined as the interpreted failure load because, beyond T_{L2}, a small increase in load gives a significant increase in displacement. Therefore, it could be adopted as a base for comparing the interpretation criteria. The statistics for the interpreted capacities and the corresponding displacements are summarized in Table 2, which includes the maximum, minimum, mean, standard deviation (SD), and coefficient of variation (COV) of the interpreted results.

The results in Table 2 show that mean interpreted load ratios of T_{DA}/T_{L2}, T_{ST}/T_{L2}, T_{TI}/T_{L2}, $T_{T\&P}/T_{L2}$, and T_{CHIN}/T_{L2} range from 0.73 to 1.20, with COV values between 0.06 and 0.20. The mean ratio of T_{L1}/T_{L2} is equal to 0.46, and a COV of 0.28 is obtained. The statistics show that the lower the capacity, the higher the COV. Meanwhile, the Davisson method presents a higher COV among all interpretation criteria. This phenomenon is similar to that reported by Chen and Chu (2012). The mean uplift displacements shown in Table 2 follow the same order trend as the uplift resistances. The mean displacements at the interpreted failure load range from 4.14 mm at T_{DA} to 6.39 mm at T_{ST} to 10.24 mm at T_{TI} to 15.72 mm at T_{L2} to > 41.11 mm for T_{CHIN}. The mean s_{L1} is 1.52 mm, which implies that the initial linear region occurs within a very small displacement. However, the COV values for the displacements are relatively large, and s_{L1} gives the largest COV of 0.80, probably because of the measurement sensitivity and initial fluctuation of the load test.

For more direct comparison of the criteria and to observe the shape effect, the normalized load–displacement curve is presented in Fig. 4. The corresponding mean ratio of each interpretation method to T_{L2} is plotted against the mean displacement. For easy observation, T_{L1}, T_{DA}, T_{ST}, T_{TI}, T_{L2}, $T_{T\&P}$, and T_{CHIN} are also marked in Fig. 4.

According to comparisons of load test results in Table 2 and Fig. 4, the Davisson, slope tangent, and tangent intersection methods yield ratio values less than 1.0, and are therefore located within the nonlinear transition between L_1 and L_2.The Terzaghi and Peck and Chin methods are beyond the end of the transition region, and the Chin method yields the highest values and even lies above the last data point recorded. Therefore, defining the failure load as T_{CHIN} results in values that are too large, likely because T_{CHIN} is based on a mathematical model that corresponds to the asymptote of the load–displacement curve.

Numerous authors consider it reasonable to interpret the failure load close to the upper limit of the nonlinear transition region, or at the beginning of the final linear region (Hirany and Kulhawy

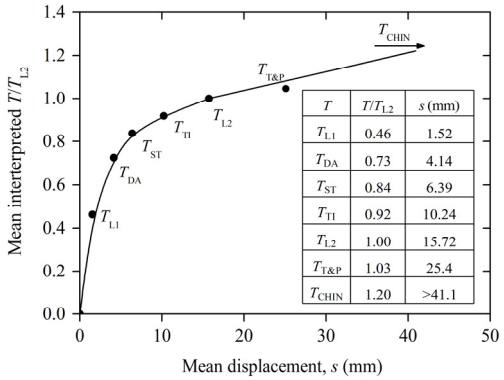

Fig. 4 Mean normalized uplift load–displacement curve for belled piers

1988, 1989, 2002, Qian *et al*. 2014b). In this study, the failure threshold T_{L2} was chosen as the measured ultimate uplift resistance because it considers the shape of the load–displacement curve and the ratio of the change in load to the change in displacement.

L_1 and L_2 are convenient reference points within the curve because these points encompass the significant regions of the curve. Using L_1 as a reference, the resistance for uplift loading can be approximated as: $T_{DA} = 1.66T_{L1}$, $T_{ST} = 1.91T_{L1}$, $T_{TI} = 2.11T_{L1}$, $T_{L2} = 2.32T_{L1}$, $T_{T\&P} = 2.33T_{L1}$, and $T_{CHIN} = 2.79T_{L1}$. These ratios can be used with caution to interrelate the methods where needed due to limited load–displacement data.

3.3 Predicted uplift resistances and capacity model statistics

For the purpose of this study, the semi-empirical method suggested by Meyerhof and Adams (1968) was used to compute the predicted uplift resistances. The failure of vertically uplifted foundations can be classified into the shallow and the deep modes, and the failure mode is determined by the depth of the foundation. In this study, the angles of internal friction φ ranged from 14.0° to 44.2°, and the values of the depth to diameter ratio ranged from 0.83 to 3.85. According to the assumptions by Meyerhof and Adams, the belled piers discussed in this study would be in shallow failure mode; therefore, the theoretical equation for their axial uplift resistances can be given by

$$T_{up} = W_f + W_s + \pi BcD + \frac{\pi}{2} s_f B\gamma_s D^2 K_u \tan\varphi \tag{1}$$

where T_{up} = predicted uplift resistance; W_f = weight of the foundation; W_s = weight of the soil; c = soil cohesion; φ = angle of soil internal friction; γ_s = unit weight of soil; D = depth of embedment; B = diameter of the foundation; K_u = nominal uplift coefficient of earth pressure on the vertical rupture surface determined as $K_u = 0.496(\varphi)^{0.18}$, where φ is in degrees; and s_f = shape factor governing the passive earth pressure on the side of a cylinder expressed by $s_f = 1 + (MD / B)$, where M is a function of φ.

By using Eq. (1), the predicted uplift resistance T_{up} can be calculated for each of the load tests. A summary of the predicted uplift resistance T_{up} is presented in Appendix D.

With the measured and predicted uplift resistances obtained as previously described, the bias factor (λ_T) for a given load test was then computed from

$$\lambda_T = T_{L2} / T_{up} \tag{2}$$

In principle, the bias factor accounts for all the sources of uncertainties (i.e., model error, systematic error, inherent spatial variability, statistical error, and load tests related errors). However, due to the level of expertise and experience of companies in charge of the load tests, measurement errors are minimized. It is likely that model error is the principal component (Dithinde *et al*. 2011, Gong *et al*. 2014). Therefore, the term model factor (M_T) instead of the bias factor (λ_T) will be used to refer to the ratio of the measured to the predicted resistance. Appendix D presents the model factor for each uplift load test, and M_T followed a normal distribution, with a mean of 1.015 and a COV of 0.285. The resistance model factor statistics would be very useful for reliability-based ULS design.

4. Normalized load–displacement behaviour

It is well known that properly normalized load–displacement curves can portray a wide variety of behaviours in a simple form, and the hyperbolic model is commonly recommended to describe these normalized load–displacement behaviours (Briaud 2007, Phoon 2008, Dithinde *et al*. 2011, Akbas and Kulhawy 2009, Qian *et al*. 2014a).

The original load–displacement curve for each load test was approximated using the hyperbolic fitting method. Two hyperbolic curve-fitting parameters, a and b, for the normalized load–displacement curve were obtained for each load test by describing the measured load–displacement curve as below

$$\frac{T}{T_{L2}} = \frac{s}{a + bs} \tag{3}$$

where T is the applied uplift load at a displacement of s, and T/T_{L2} is the normalized load in which the applied load is normalized by the failure load interpreted from the L_1–L_2 method. Note that the curve-fitting parameters are physically meaningful, with the reciprocals of a and b being equal to the initial slope and asymptotic value, respectively.

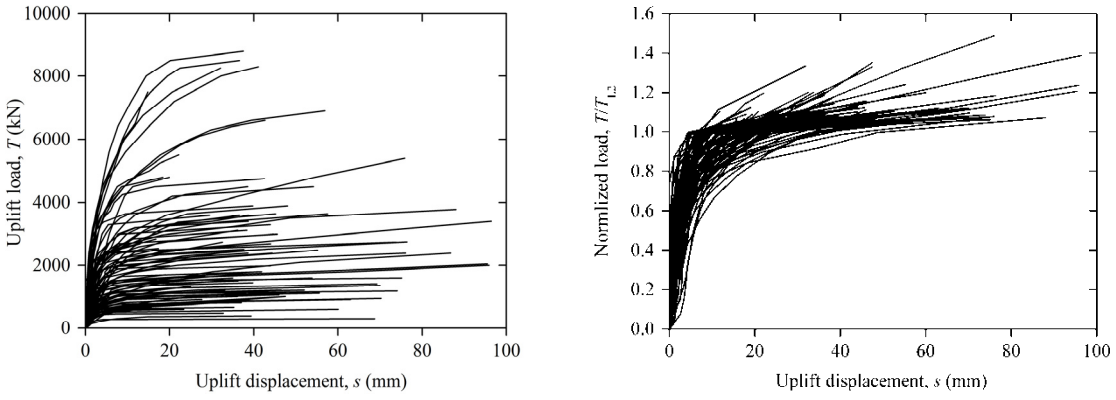

(a) Original load–displacement curves (b) Normalized load–displacement curves

Fig. 5 Original versus normalized load–displacement curves

Fig. 5 shows the original and normalized load–displacement curves. Comparison of the two sets of curves shows that normalizing the load–displacement curves reduces scattering within the curves compared to the originally measured load–displacement curves.

The hyperbolic curve-fitting parameters a and b for each measured load–displacement curve are provided in Appendix D. To avoid bias in the reliability calculations, the dependence, or correlation between model parameters, must be incorporated in the simulations (Phoon and Kulhawy 2008, Dithinde *et al*. 2011, Uzielli and Mayne 2012, Tang *et al*. 2013, Huffman and Stuedlein 2014). It is therefore natural to consider a, or b as a random variable. Fig. 6(a) shows the scatter plots of a and b for all the belled piers. The scatter plot indicates that a and b are not statistically independent. Mathematically, the simplest measure of statistical dependence is the Pearson product-moment correlation

$$\rho_{ab} = \frac{\sum_{i=1}^{N}(a_i - \overline{a})(b_i - \overline{b})}{\sqrt{\sum_{i=1}^{N}(a_i - \overline{a})^2 \sum_{i=1}^{N}(b_i - \overline{b})^2}} \tag{4}$$

where (a_i, b_i) denotes a pair of a and b for the normalized load–displacement curve obtained by Eq. (3) for each test, and $\overline{a}$ and $\overline{b}$ are the sample means.

The Pearson correlation coefficient ($\rho_{a,b}$) is reported in Fig. 6(a), which is negative with a value of −0.724. This conclusion is consistent with that reported by Phoon (2008), Phoon *et al*. (2007), Dithinde *et al*. (2011), and Qian *et al*. (2014a). Physically, this negative correlation implies that the initial slope (1/a) tends to increase when the asymptotic value (1/b) decrease or vice-versa for the normalized load–displacement curve.

According to Eq. (3), each pair of (a_i, b_i) can describe a single load–displacement, but the hyperbolic curve-fitting parameters a and b vary with soil properties and foundation dimensions. Therefore, an empirical approach is required to determine the hyperbolic normalized load–displacement relationship of Eq (3), and the explicit forms of a and b could be determined using the confidence limit method.

Fig. 6(b) illustrates the statistical distributions of hyperbolic curve-fitting parameters a and b.

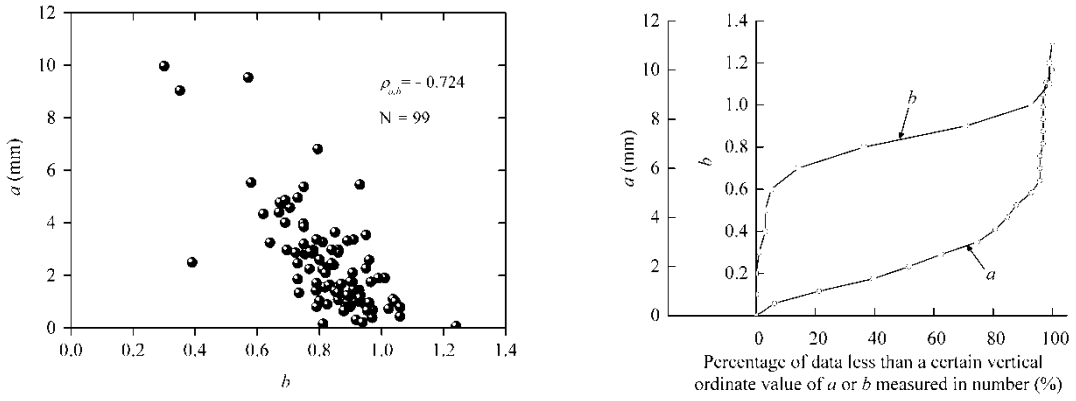

(a) Scatter plots of a and b (b) Statistical distributions of a and b

Fig. 6 Probability distributions of hyperbolic curve-fitting parameters a and b

Table 3 Summary of statistics for hyperbolic curve-fitting parameters *a* and *b*

Parameter	Minimum	Mean	Maximum	SD	COV	95% C.L.
a (mm)	0.074	2.427	9.970	1.882	0.775	5.346
b	0.300	0.831	1.240	0.148	0.178	1.034

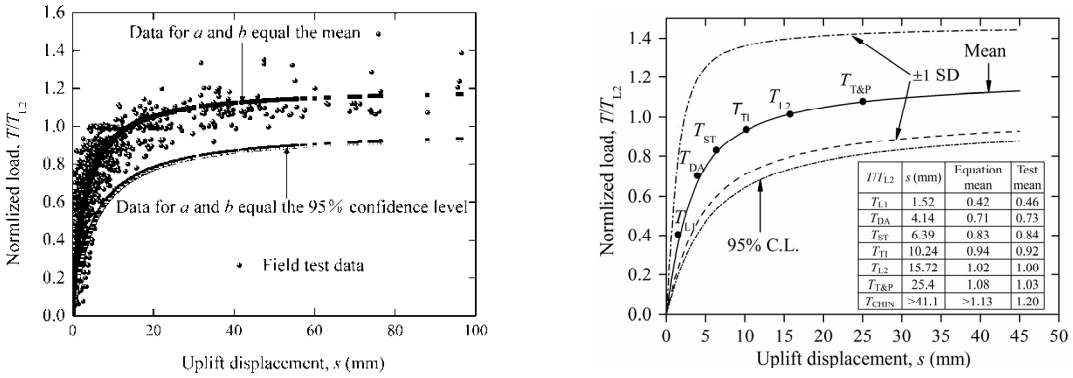

(a) Comparison of uplift load-displacement relationships with field test data

(b) Uplift load-displacement relationship for design of belled piers

Fig. 7 Normalized uplift load versus the mean displacement

The ordinate represents a curve-fitting parameter *a* or *b*, and the abscissa represents the percentage of data less than a certain vertical ordinate value of *a* or *b* measured in number. According to Fig. 6(b), the parameters *a* and *b* can be characterized by different confidence limit levels. Table 3 summarizes the statistics for the hyperbolic curve-fitting parameters *a* and *b*. In practice, the curve-fitting parameters *a* and *b* at the 50% confidence limit level (mean) and the 95% confidence limit level appear to be typical and may have different implications.

Fig. 7(a) shows comparisons between the field test data and the evaluated load–displacement responses obtained from Eq. (3) when the curve-fitting parameters *a* and *b* are equal to the mean and the 95% confidence limit level. Fig. 7(a) indicates that the mean data more closely represents the actually measured load–displacement points. In general, the field tests showed a substantially stiffer load–displacement response than the data obtained at the 95% confidence limit level. Physically, the use of these data means that, on average, 95% of all the test data will have a stiffer load–displacement response than that shown.

The resulting mean curve described by Eq. (3), which indicates the normalized load versus the corresponding displacement, is illustrated as a solid line in Fig. 7(b). Three dashed curves, which correspond to plus and minus one SD from the mean (±1 SD) and the 95% confidence limit level (95% C.L.), represent the uncertainty associated with the normalized curve. The mean values between T_{L2} and T_{L1}, T_{DA}, T_{ST}, T_{TI}, T_{L2} and $T_{T\&P}$, as well as the values of s_{L1}, s_{DA}, s_{ST}, s_{TI}, s_{L2}, and s_{L2}, which were obtained from the load test statistical analyses, are shown on Fig. 7(b). The actual points of T_{L1}, T_{DA}, T_{ST}, T_{TI}, T_{L2}, $T_{T\&P}$, and T_{CHIN}, which were obtained using Eq. (3) corresponding to the mean displacement values from the test statistics, are also marked on Fig. 7(b). The differences between the field tests and those obtained using Eq. (3) are relatively small, with a value 2%-10%, because the mean hyperbolic curve is similar to the actual data points for most of load tests, as shown in Fig. 7(a).

5. Derivation of serviceability limit state (SLS) model factor statics

For the SLS, it is most convenient to capture the uncertainties in the nonlinear load–displacement curves by using the hyperbolic equation (i.e., Eq. (3)). Therefore, the permissible load (T_a) and the resulting permissible displacement (s_a) can be expressed as follows

$$\frac{T_a}{T_{L2}} = \frac{s_a}{a + bs_a} \tag{5}$$

$$\text{Let } \frac{s_a}{a + bs_a} = M_s \tag{6}$$

$$T_a = M_s T_{L2} \tag{7}$$

where M_s = SLS model factor and the other symbols are as defined previously.

As defined by Eqs. (2) and (6), M_T and M_s could be considered as random variables. The statistics for the former are meant for ULS, while the statistics for the latter are functions of the permissible displacement (s_a), and the mean (u_{Ms}) and COV (COV_{Ms}) can be estimated as follows (Phoon and Kulhawy 2008, Dithinde *et al*. 2011)

$$\mu_{M_s} = \frac{s_a}{\mu_a + \mu_b s_a} \tag{8}$$

$$\text{COV}_{M_s} = \frac{\sqrt{\sigma_a^2 + s_a^2\sigma_b^2 + 2s_a\rho_{ab}\sigma_a\sigma_b}}{\mu_a + \mu_b s_a} \tag{9}$$

where μ_a and μ_b = mean of a and b, respectively, and σ_a and σ_b = standard deviation of a and b, respectively.

Using Eqs. (8) and (9) in conjunction with the hyperbolic parameter statistics (Table 3) as well as their Pearson correlation coefficient ($\rho_{a,b}$) in Fig. 6(a), M_s statistics can be obtained for a given allowable displacement. The resulting SLS model factor uncertainty statistics will vary with the given allowable displacements, as shown in Table 4.

It should be pointed out that the interpreted uplift resistance T_{L2} using the L_1–L_2 method for belled piers is generally unavailable at the design stage; therefore, Eq. (7) should be modified as follows for the reliability calibration

Table 4 Variations of combined ULS and SLS model factor statistics

s_a	a (mm)		b		ρ_{ab}	M_s		M_T		M_sM_T	
(mm)	μ_a	σ_a	μ_b	σ_b		u_{Ms}	COV_{Ms}	u_{MT}	COV_{MT}	u_{MsMT}	COV_{MsMT}
5.0						0.760	0.219			0.771	0.359
10.0						0.931	0.121			0.945	0.310
15.0	2.427	1.882	0.831	0.148	-0.724	1.007	0.104	1.015	0.285	1.022	0.303
20.0						1.050	0.108			1.066	0.305
25.0						1.077	0.115			1.093	0.307

$$T_a = (M_s M_T) T_{up} \tag{10}$$

The important point here is that uncertainties in ULS (manifested by M_T) must be included if T_a is calculated from T_{up} (determined by Eq. (1)) . If we assume that M_s and M_T are uncorrelated, the combined statistics ($M_s M_T$) can be computed as

$$\mu_{M_s M_T} = \mu_{M_s} \mu_{M_T} \tag{11}$$

$$\mathrm{COV}_{M_s M_T} = \sqrt{\mathrm{COV}_{M_s}^2 + \mathrm{COV}_{M_T}^2} \tag{12}$$

Table 4 shows the variations of the combined ULS and SLS model factor statistics for different permissible displacements. These performances on the ULS and SLS statistics would be directly applicable to reliability calibration of resistance factors (for ULS) and deformation factors (for SLS) for designs of belled piers.

The approaches and the results in this study were practical and grounded realistically on the load tests of belled piers with minimal assumptions, which can be used as a convenient design tool to simultaneously consider both the resistance and the displacement and can be served to extend the early contributions for reliability-based ULS and SLS designs.

7. Conclusions

Based on 99 full-scale uplift load tests conducted on belled piers at 22 sites in China, the following conclusions can be drawn.

(1) The uplift load–displacement curves of belled piers could schematically be simplified into three distinct regions: initial linear, nonlinear transition, and final linear region; therefore, the failure resistance should be interpreted by uplift interpretation criteria as done in other studies. The Davisson, slope tangent, and tangent intersection methods were located within the nonlinear transition region between L_1 and L_2. The Terzaghi and Peck and Chin methods were beyond the end of the transition region, and the Chin method yields the highest values.

(2) The L_1–L_2 method considers the shape of the load–displacement curve and the ratio of the change in load to the change in displacement, and could be preferred to interpret the uplift resistance. The failure threshold T_{L2} could be chosen as the measured ultimate uplift resistance for belled piers. The capacity model factor, M_T, defined as the ratio of the interpreted uplift resistance (L_1–L_2 method) and the predicted resistance (Meyerhof and Adams design formula), followed a normal distribution, with a mean of 1.015 and a COV of 0.285. The resistance model factor statistics were useful for reliability-based ULS design.

(3) L_1 and L_2 are convenient reference points within the curve because these points encompass the significant regions of the curve. Using L_1 as a reference, the resistance for uplift loading can be given as $T_{DA} = 1.66T_{L1}$, $T_{ST} = 1.91T_{L1}$, $T_{TI} = 2.11T_{L1}$, $T_{L2} = 2.32T_{L1}$, $T_{T\&P} = 2.33T_{L1}$, and $T_{CHIN} = 2.79T_{L1}$. Using L_2, the resistance can be approximated as $T_{L1} = 0.46T_{L2}$, $T_{DA} = 0.73T_{L2}$, $T_{ST} = 0.84T_{L2}$, $T_{TI} = 0.92T_{L2}$, $T_{T\&P} = 1.03T_{L2}$, and $T_{CHIN} = 1.20T_{L2}$. These ratios can be used with caution to interrelate the methods where needed due to

limited load–displacement data for belled piers.

(4) The original uplift load–displacement behaviour of the belled piers could be normalized and expressed by the hyperbolic model as done in other studies. Normalizing the load–displacement curves significantly reduced scattering in the curves. The hyperbolic curve-fitting parameters *a* and *b* were statistically correlated, and the Pearson correlation coefficient of those was negative. These conclusions were also consistent with those in previous studies.

(5) Explicit hyperbolic curve-fitting parameters *a* and *b* were obtained for axial uplift belled piers at different confidence limit levels. The uncertainty associated with the normalized load–displacement curves could also be represented by the curves which corresponded to the explicit hyperbolic curve-fitting parameters *a* and *b*.

(6) It was convenient to obtain the uncertainties in the nonlinear load–displacement curve by using the hyperbolic equation for the SLS design. The resulting SLS model factor, M_s, statistics can be computed for a given allowable displacement, and M_s statistics varied with the allowable displacements.

(7) The variations of the combined ULS and SLS model factor statistics should be considered for the reliability-based designs, which can be used as a convenient design tool to simultaneously consider both the resistance and displacement and can be served to extend the early contributions for reliability-based ULS and SLS designs.

It should be noted that the results discussed in this study are general behaviours applicable for the belled piers in shallow failure mode, and any extrapolation of these results to other deep foundations is not recommended.

Acknowledgments

The authors wish to acknowledge the support provided by the National Natural Science Foundation of China (No. 51208480). Also, the authors wish to thank the State Grid Corporation of China for the support of the projects (No. GCB17201200123, No. GCB17201200089). The authors also appreciate the reviewers' excellent comments, which have improved the quality of this paper.

References

Akbas, S.O. and Kulhawy, F.H. (2009), "Axial compression of footings in cohesionless soils. I: Load–settlement behavior", *J. Geotech. Geoenviron. Eng.*, **135**(11), 1562-1574.

Briaud, J.L. (2007), "Spread footings in sand: load settlement curve approach", *J. Geotech. Geoenviron. Eng.*, **133**(8), 905-920.

Chen, J.R. (1998), "Case history evaluation of axial behavior of augered-cast-in-place piles and pressure-injected footings", M.S. Thesis; Department of Civil and Environmental Engineering, Cornell University, Ithaca, NY, USA.

Chen, J.R. (2004), "Axial behavior of drilled shafts in gravelly soils", Ph.D. Thesis; Department of Civil and Environmental Engineering, Cornell University, NY, USA.

Chen, J.R. and Kulhawy, F.H. (2002), "Axial uplift behavior of pressure-injected footings in cohsionless soil", In: *Deep Foundations 2002* (M.W. O'Neill and F.C. Townsend Eds.), GSP 116; Reston, VA, USA, pp. 1275-1289.

Chen, J.R. and Kulhawy, F.H. (2003), "Significance of construction effects on uplift behavior of drilled foundations", *Proceedings of the 12th Asian Regional Conference on Soil Mechanics and Geotechnical Engineering*, Singapore, August, pp. 591-594.
Chen, Y.J. and Chu, T.H. (2012), "Evaluation of uplift interpretation criteria for drilled shafts in gravely soils", *Can. Geotech. J.*, **49**(1), 70-77.
Chen, Y.J. and Fang, Y.C. (2009), "Critical evaluation of compression interpretation criteria for drilled shafts", *J. Geotech. Geoenviron. Eng.*, **135**(8), 1056-1069.
Chen, Y.J., Chang, H.W. and Kulhawy, F.H. (2008), "Evaluation of uplift interpretation criteria for drilled shaft capacity", *J. Geotech. Geoenviron. Eng.*, **134**(10), 1459-1468.
Chen, Y.J and Lee, Y.H. (2010), "Evaluation of lateral interpretation criteria for drilled shaft capacity", *J. Geotech. Geoenviron. Eng.*, **136**(8), 1124-1136.
Chen, Y.J., Lin, S.W. and Kulhawy, F.H. (2011), "Evaluation of lateral interpretation criteria for rigid drilled shafts", *Can. Geotech. J.*, **48**(4), 634-643.
Chen, Y.J., Liao, M.R., Lin, S.S., Huang, J.K. and Marcos, M.C.M. (2014), "Development of an integrated Web-based system with a pile load test database and pre-analyzed data", *Geomech. Eng., Int. J.*, **7**(1), 37-53.
Chin, F.K. (1970), "Estimation of the ultimate load of piles not carried to failure", *Proceedings of the 2nd Southeast Asian Conference on Soil Engineering*, Singapore, June, pp. 81-90.
Chin, F.K. (1978), "Diagnosis of ple condition", *Geotech. Eng., Int. J.*, **9**(2), 85-104.
Ching, J.Y. and Chen, J.R. (2010), "Predicting displacement of augered cast-in-place piles based on load test database", *Struct. Safety*, **32**(6), 372-383.
Davisson, M.T. (1972), "High capacity piles", *Proceedings of the Lecture Series on Innovations in Foundation Construction*, Illinois Section, Chicago, IL, USA, March, pp. 81-112.
DeBeer, E.E. (1970), "Experimental determination of the shape factors and bearing capacity factors of sand", *Géotechnique*, **20**(4), 387-411.
Dithinde, M., Phoon, K.K., Wet, M.D. and Retief, J.V. (2011), "Characterization of model uncertainty in the static pile design formula", *J. Geotech. Geoenviron. Eng.*, **137**(1), 70-85.
Fuller, F.M. and Hoy, H.E. (1970), "Pile load tests including quick load test method, conventional methods, and interpretations", Research Record 333; *Highway Research Board*, Washington, D.C., USA, pp. 74-86.
Gong, W.P., Khoshnevisan, S. and Juang, C.H. (2014), "Gradient-based design robustness measure for robust geotechnical design", *Can. Geotech. J.*, **51**(11), 1331-1342.
Hirany, A. and Kulhawy, F.H. (1988), "Conduct and interpretation of load tests on drilled shaft foundations: Detailed guidelines", Report No. EPRI EL-5915; Electric Power Research Institute, Palo Alto, CA, USA, pp. 272-273.
Hirany, A. and Kulhawy, F.H. (1989), "Interpretation of load tests on drilled shafts. II: axial uplift", In: *Foundation Engineering*: *Current Principles and Practices*, (F.H. Kulhawy Eds.), GSP 22; New York, NY, USA, pp. 1150-1159.
Hirany, A. and Kulhawy, F.H. (2002), "On the interpretation of drilled foundation load test results", In: *Deep Foundations*, (M.W. O'Neill and F.C. Townsend Eds.), GSP 22; Reston, VA, USA, pp. 1018-1028.
Housel, W.S. (1966), "Pile load capacity: Estimates and test results", *J. Soil Mech. Found. Div.*, **92**(SM4), 1-30.
Huffman, J. and Stuedlein, A. (2014), "Reliability-based serviceability limit state design of spread footings on aggregate pier reinforced clay", *J. Geotech. Geoenviron. Eng.*, **140**(10), 1-11.
Jeon, S.S. and Kulhawy, F.H. (2001), "Evaluation of axial compression behavior of micropiles", *Proceedings of Foundation and Ground Improvement*, (T.L. Brandon Eds.), GSP 113; Reston, VA, USA, pp. 460-471.
Kulhawy, F.H. and Jeon, S.S. (1999), "Some observations on axial compression behavior of micropiles", *Proceedings of the 2nd International Workshop on Micropiles*, Ube, Japan, October, pp. 89-92.
Li, D.Q., Tang, X.S., Phoon, K.K., Chen, Y.F. and Zhou, C.B. (2013), "Bivariate simulation using copula and its application to probabilistic pile settlement analysis", *Int. J. Numer. Anal. Method. Geomech.*, **37**(6), 597-617.

Marcos, M.C.M., Chen, Y.J. and Kulhawy, F.H. (2013), "Evaluation of compression load test interpretation criteria for driven precast concrete pile capacity", *KSCE J. Civ. Eng.*, **17**(5), 1008-1022.

Meyerhof, G.G. and Adams, J.I. (1968), "The ultimate uplift capacity of foundations", *Can. Geotech. J.* **5**(4), 225-244.

O'Rourke, T.D. and Kulhawy, F.H. (1985), "Observations on load tests on drilled shafts", In: *Drilled Piers and Caissons II*, (C.N. Baker Eds.), New York, NY, USA, pp. 113-128.

Phoon, K.K. (2005), "Reliability-based design incorporating model uncertainties", *Proceedings of the 3rd International Conference on Geotechnical Engineering and the 9th Yearly Meeting of Indonesian Society for Geotechnical Engineering*, Diponegoro University, Semorang, Indonesia, December, pp. 191-203.

Phoon, K.K. (2008), "Numerical recipes for reliability analysis—A primer", Chapter 1, In: *Reliability-Based Design in Geotechnical Engineering*: *Computations and Applications*, Taylor & Francis, London, UK, pp. 1-75.

Phoon, K.K., Chen, J.R. and Kulhawy, F.H. (2007), "Probabilistic hyperbolic models for foundation uplift movement", *Proceedings of the Probabilistic Applications in Geotechnical Engineering*, (K.K. Phoon, G.G. Fenton, E.F. Glynn, C.H. Juang, D.V. Griffiths, T.F. Wolff and L. Zhang Eds.), GSP 170; Reston, VA, USA, pp. 1-12. [CD-ROM]

Phoon, K.K. and Kulhawy, F.H. (2008), "Serviceability limit state reliability-based design", Chapter 9, In: *Reliability-Based Design in Geotechnical Engineering*: *Computations and Applications*, Taylor and Francis, London, UK, pp. 344-384.

Qian, Z.Z, Lu, X.L. and Yang, W.Z. (2014a), "Axial uplift behavior of drilled shafts in Gobi gravel", *Geotech. Test. J.*, **37**(2), 205-217.

Qian, Z.Z, Lu, X.L., Yang, W.Z. and Cui, Q. (2014b), "Behaviour of micropiles in collapsible loess under tension or compression load", *Geomech. Eng., Int. J.*, **7**(5), 477-493.

Stewart, H.E. and Kulhawy, F.H. (1990), "Field evaluation of grillage foundation uplift capacity", Report No. EPRI EL-6965; Electric Power Research Institute, Palo Alto, CA, USA.

Tang, X.S., Li, D.Q., Rong, G., Phoon, K.K. and Zhou, C.B. (2013), "Impact of copula selection on geotechnical reliability under incomplete probability information", *Comput. Geotech.*, **49**, 264-278.

Terzaghi, K. and Peck, R.B. (1967), *Soil Mechanics in Engineering Practice*, (2nd Ed.), Wiley, New York, NY, USA.

Tomlinson, M.J. (1977), *Pile Design and Construction Practice* (*A Viewpoint Publication*), Cement & Concrete Association of Great Britain, London, UK.

Uzielli, M. and Mayne, P. (2012), "Load-displacement uncertainty of vertically loaded shallow footings on sands and effects on probabilistic settlement", *Georisk*, **6**(1), 50-69.

CC

Appendix A

Table A Test location and soil description

Site No.	Test location	Soil description
1	Anhua County, Hunan Province	Silty clay
2	Yiyang City, Hunan Province	Silty sand over weathered slate
3	Longyou County, Zhejiang Province	Weathered pelitic sandstone
4	Qitaihe City, Heilongjiang Province	Residual soil over silty clay
5	Xintai County, Hebei Province	Silty clay over silt
6	Changzhi City, Shanxi Province	Silty clay over silt
7	Fushun City, Liaonin Province	Sandy silt
8	Kunming City, Yunnan Province	Strong weathered mudstone
9	Luohu Distict, Shenzhen City, Guangdong Province	Sandy silt
10	Xuanchen City, Anhui Province	Silty clay
11	Yejiashan, Jiangxi Province	Silty clay
12	Jiujiang City, Jiangxi Province	Silty clay over weathered mudstone
13	Gangu County, Gansu Province	Fine loessial silt and clay
14	Dingxi City, Gansu Province	Fine loessial silt and clay
15	Yuzhong County, Gansu Province	Fine loessial silt and clay
16	Gaotai County, Gansu Province	Medium to dense Gobi gravel
17	Shandan County, Gansu Province	Medium to dense Gobi gravel
18	Jinchang City, Gansu Province	Medium to dense Gobi gravel
19	Jiuquan City, Gansu Province	Medium to dense Gobi gravel
20	Salt Lake near Dabancheng Town, Urmmqi, Xinjiang Uygur Autonomous Region	Loose Gobi gravel
21	Erlidian near Dabancheng Towen, Urmmqi, Xinjiang Uygur Autonomous Region	Medium dense Gobi gravel
22	Wild Zoo near Dabancheng Towen, Urmmqi, Xinjiang Uygur Autonomous Region	Medium dense Gobi gravel

Appendix B

Table B Dimensions of the belled piers and soil properties.

Case No.	D (m)	B (m)	b (m)	t (m)	θ (°)	e (m)	c^a (kPa)	φ^a (°)	γ_s (kN/m^3)
1/1	4.10	2.20	1.20	0.20	32.0	0.20	41.3	27.2	18.6
1/2	4.10	2.20	1.20	0.20	32.0	0.20	41.3	27.2	18.6
1/3	4.10	2.20	1.20	0.20	32.0	0.20	41.3	27.2	18.6
2/1	3.50	2.20	1.20	0.20	32.0	0.20	48.0	14.0	18.0
2/2	3.50	2.20	1.20	0.20	32.0	0.20	48.0	14.0	18.0
3/1	2.00	1.80	0.80	0.20	39.8	0.30	63.9	41.7	19.4
3/2	2.00	1.80	0.80	0.20	39.8	0.30	44.7	27.7	18.2
3/3	2.00	1.80	0.80	0.20	39.8	0.30	43.7	27.0	18.2
3/4	2.00	2.10	0.80	0.20	45.0	1.50	44.7	27.7	18.2
3/5	2.00	2.10	0.80	0.20	45.0	1.50	48.2	30.2	18.5
3/6	2.00	2.10	0.80	0.20	45.0	1.50	62.8	40.9	19.4
4/1	2.30	2.10	1.00	0.20	34.5	0.20	26.9	40.0	18.2
4/2	2.30	2.10	1.00	0.20	34.5	0.20	26.9	40.0	18.2
4/3	2.80	2.30	1.00	0.20	35.8	0.20	18.6	28.0	19.0
4/4	2.80	2.30	1.00	0.20	35.8	0.20	18.6	28.0	19.0
5/1	3.30	2.10	0.90	0.20	33.7	0.20	26.8	19.1	18.4
5/2	3.30	2.10	0.90	0.20	33.7	0.20	26.8	19.1	18.4
5/3	2.90	2.40	1.10	0.20	35.8	0.20	26.8	19.1	18.4
5/4	2.90	2.40	1.10	0.20	35.8	0.20	26.8	19.1	18.4
6/1	2.60	1.60	0.80	0.20	33.7	0.20	41.8	30.4	16.3
6/2	4.20	2.00	1.00	0.20	33.7	0.20	41.8	30.4	16.3
6/3	5.70	2.50	1.00	0.20	34.3	0.20	41.8	30.4	16.3
7/1	2.80	2.30	1.00	0.20	35.8	0.05	8.8	37.1	18.8
7/2	2.80	2.30	1.00	0.20	35.8	0.05	8.8	37.1	18.8
7/3	2.80	2.30	1.00	0.20	35.8	0.05	8.8	37.1	18.8
7/4	2.80	2.30	1.00	0.20	35.8	0.05	8.8	37.1	18.8
8/1	4.10	2.00	1.00	0.30	45.0	1.00	12.8	20.7	16.0
9/1	2.00	2.40	1.20	0.20	36.9	0.20	33.6	30.4	18.4
9/2	3.00	2.40	1.20	0.20	36.9	0.20	33.6	30.4	18.4
10/1	2.40	2.40	1.20	0.20	36.9	0.20	32.0	19.0	18.8
10/2	3.40	2.40	1.20	0.20	36.9	0.20	32.0	19.0	18.8
10/3	4.40	2.40	1.20	0.20	36.9	0.20	32.0	19.0	18.8
11/1	4.00	2.10	1.00	0.20	34.5	0.20	9.4	32.9	19.3
11/2	5.00	2.10	1.00	0.20	34.5	0.20	9.4	32.9	19.3
11/3	6.00	2.10	1.00	0.20	34.5	0.20	9.4	32.9	19.3
12/1	4.00	2.50	1.40	0.20	34.5	0.20	13.8	17.3	17.7
12/2	4.00	2.10	1.00	0.20	34.5	0.20	13.8	17.3	17.7
12/3	4.00	1.50	1.00	0.20	17.4	0.20	13.8	17.3	17.7

Table B Continued

Case No.	D (m)	B (m)	b (m)	t (m)	θ (°)	e (m)	c^a (kPa)	φ^a (°)	γ_s (kN/m^3)
13/1	2.00	1.20	0.90	0.20	14.0	0.20	15.2	23.2	15.4
13/2	3.10	1.90	1.20	0.20	30.3	0.20	15.2	23.2	15.4
13/3	4.30	2.70	1.50	0.20	45.0	0.20	15.2	23.2	15.4
13/4	3.20	1.50	1.20	0.20	14.0	0.20	15.2	23.2	15.4
13/5	4.60	2.20	1.50	0.20	30.3	0.20	15.2	23.2	15.4
13/6	4.40	2.10	0.90	0.20	45.0	0.20	15.2	23.2	15.4
13/7	4.70	1.80	1.50	0.20	14.0	0.20	15.2	23.2	15.4
13/8	4.20	1.60	0.90	0.20	30.3	0.20	15.2	23.2	15.4
13/9	6.20	2.40	1.20	0.20	45.0	0.20	15.2	23.2	15.4
13/10	7.70	2.00	1.00	0.20	39.8	0.20	15.2	23.2	15.4
13/11	7.70	3.00	1.50	0.20	51.3	0.20	15.2	23.2	15.4
14/1	3.70	2.00	1.00	0.20	39.8	0.20	21.5	26.8	13.2
14/2	5.20	2.00	1.00	0.20	39.8	0.20	21.5	26.8	13.2
14/3	7.70	2.00	1.00	0.20	39.8	0.20	21.5	26.8	13.2
15/1	7.70	2.00	1.00	0.20	39.8	0.20	13.3	32.8	13.3
16/1	1.92	1.01	0.80	0.20	9.9	0.20	10.5	41.4	20.1
16/2	2.85	1.64	1.20	0.20	20.1	0.20	10.5	41.4	20.1
16/3	3.84	2.29	1.60	0.20	29.9	0.20	10.5	41.4	20.1
16/4	3.93	1.41	1.20	0.20	9.9	0.20	10.5	41.4	20.1
16/5	5.49	2.04	1.60	0.20	20.1	0.20	10.5	41.4	20.1
16/6	4.13	1.49	0.80	0.20	29.9	0.20	10.5	41.4	20.1
16/7	6.74	1.81	1.60	0.20	9.9	0.20	10.5	41.4	20.1
16/8	4.73	1.24	0.80	0.20	20.1	0.20	10.5	41.4	20.1
16/9	7.02	1.89	1.20	0.20	29.9	0.20	10.5	41.4	20.1
17/1	1.92	1.01	0.80	0.20	9.9	0.20	23.0	43.3	21.0
17/2	2.85	1.64	1.20	0.20	20.1	0.20	23.0	43.3	21.0
17/3	3.84	2.29	1.60	0.20	29.9	0.20	23.0	43.3	21.0
17/4	3.93	1.41	1.20	0.20	9.9	0.20	23.0	43.3	21.0
17/5	5.49	2.04	1.60	0.20	20.1	0.20	23.0	43.3	21.0
17/6	4.13	1.49	0.80	0.20	29.9	0.20	23.0	43.3	21.0
17/7	6.74	1.81	1.60	0.20	9.9	0.20	23.0	43.3	21.0
17/8	4.73	1.24	0.80	0.20	20.1	0.20	23.0	43.3	21.0
17/9	7.02	1.89	1.20	0.20	29.9	0.20	23.0	43.3	21.0
18/1	1.92	1.01	0.80	0.20	9.9	0.20	14.7	44.2	21.4
18/2	2.85	1.64	1.20	0.20	20.1	0.20	14.7	44.2	21.4
18/3	3.84	2.29	1.60	0.20	29.9	0.20	14.7	44.2	21.4
18/4	3.93	1.41	1.20	0.20	9.9	0.20	14.7	44.2	21.4
18/5	5.49	2.04	1.60	0.20	20.1	0.20	14.7	44.2	21.4
18/6	4.13	1.49	0.80	0.20	29.9	0.20	14.7	44.2	21.4

Table B Continued

Case No.	D (m)	B (m)	b (m)	t (m)	θ (°)	e (m)	c^a (kPa)	φ^a (°)	γ_s (kN/m^3)
18/7	6.74	1.81	1.60	0.20	9.9	0.20	14.7	44.2	21.4
18/8	4.73	1.24	0.80	0.20	20.1	0.20	14.7	44.2	21.4
18/9	7.02	1.89	1.20	0.20	29.9	0.20	14.7	44.2	21.4
19/1	2.25	1.20	0.80	0.20	18.4	0.20	21.7	40.0	20.8
19/2	2.80	1.23	0.84	0.20	18.0	0.20	21.7	40.0	20.8
19/3	3.75	1.20	0.80	0.20	18.4	0.20	21.7	40.0	20.8
19/4	3.40	1.40	1.05	0.20	16.3	0.20	21.7	40.0	20.8
19/5	4.95	1.60	1.05	0.20	24.6	0.20	21.7	40.0	20.8
19/6	4.28	1.80	1.25	0.20	24.6	0.20	21.7	40.0	20.8
19/7	5.00	1.85	1.30	0.20	24.6	0.20	21.7	40.0	20.8
20/1	2.74	1.56	1.00	0.20	25.0	0.20	15.6	42.1	17.8
20/2	5.16	1.36	0.80	0.20	25.0	0.20	15.6	42.1	17.8
21/1	2.08	1.12	0.80	0.20	14.9	0.20	16.5	43.6	20.9
21/2	2.74	1.56	1.00	0.20	25.0	0.20	16.5	43.6	20.9
21/3	3.71	2.21	1.20	0.20	40.1	0.20	16.5	43.6	20.9
21/4	3.70	1.32	1.00	0.20	14.9	0.20	16.5	43.6	20.9
21/5	4.80	1.76	1.20	0.20	25.0	0.20	16.5	43.6	20.9
21/6	4.92	1.81	0.80	0.20	40.1	0.20	16.5	43.6	20.9
21/7	5.73	1.52	1.20	0.20	14.9	0.20	16.5	43.6	20.9
21/8	5.16	1.36	0.80	0.20	25.0	0.20	16.5	43.6	20.9
21/9	7.42	2.01	1.00	0.20	40.1	0.20	16.5	43.6	20.9
22/1	4.90	1.80	1.20	0.20	26.6	0.20	20.1	40.6	21.1

[a] Soil cohesion c and friction angle φ were obtained from direct shear tests.

Appendix C

Table C Interpreted loads and displacements for belled piers in axial uplift

Case No.	Interpreted uplift resistance, T[a] (kN), and the displacement, s[b, c] (mm)												
	T_{L1}	s_{L1}	T_{DA}	s_{DA}	T_{ST}	s_{ST}	T_{TI}	s_{TI}	T_{L2}	s_{L2}	$T_{T\&P}$	T_{CHIN}	s_{CHIN}
1/1	1082	0.60	2297	4.08	2404	5.30	2299	4.13	2580	8.70	–[d]	2979	>16.7[e]
1/2	1650	0.63	2350	4.05	2369	4.30	2350	4.20	2410	5.00	–	2598	>17.3
1/3	847	0.21	2280	4.07	2290	4.17	2281	3.90	2562	8.90	–	2741	>13.2
2/1	1299	0.40	2050	4.18	2052	4.40	2104	5.30	2289	10.70	2561	2694	30.32
2/2	970	0.01	1847	3.79	1845	3.78	1929	5.90	2016	9.20	2180	2446	50.13
3/1	383	1.24	767	3.87	867	5.07	987	7.00	1359	15.40	–	1751	>20.8
3/2	288	0.40	613	3.85	621	4.41	677	6.91	776	17.72	815	868	>28.9
3/3	317	1.37	616	3.82	851	6.91	794	5.80	926	10.41	–	1314	>12.1
3/4	326	0.60	665	3.87	743	5.21	868	8.80	907	10.60	962	1092	>46.1
3/5	309	1.80	432	3.87	524	6.83	621	10.30	686	14.20	748	903	>33.8
3/6	480	0.50	770	3.95	801	4.74	956	9.10	1228	18.67	1320	1326	>25.3
4/1	496	0.95	906	3.91	1046	5.65	990	4.90	1089	6.48	–	1379	>11.7
4/2	372	2.70	440	3.86	644	8.11	812	14.60	1078	33.70	980	1373	>46.2
4/3	727	0.70	1195	4.01	1223	4.81	1336	10.20	1406	15.60	1448	1526	>36.2
4/4	515	0.60	766	3.99	795	4.73	939	9.60	1102	20.90	1131	1220	>33.1
5/1	331	1.50	505	3.86	657	10.97	565	6.50	741	18.20	756	920	>38.9
5/2	494	4.90	390	3.98	657	10.75	646	9.99	740	18.20	795	1120	>47.5
5/3	281	0.50	539	3.82	566	4.77	639	7.50	752	15.20	825	1015	>47.5
5/4	296	1.30	515	3.88	574	6.38	587	6.95	728	19.20	778	926	>36.3
6/1	310	0.20	509	3.99	508	4.21	470	1.50	492	2.50	–	654	>15.6
6/2	913	0.68	1378	3.98	1409	4.81	1400	4.63	1511	7.48	–	1753	>19.1
6/3	1200	5.89	603	4.07	1336	9.31	1363	9.80	1421	13.86	1516	1961	>35.1
7/1	317	0.43	772	3.98	830	4.66	1078	13.31	1107	15.29	1128	1239	>51.9
7/2	413	0.64	743	3.99	800	4.97	966	12.23	1000	14.76	1025	1127	>55.6
7/3	414	0.86	745	3.91	834	5.72	968	10.64	1004	12.37	1031	1134	>47.6
7/4	496	1.67	720	4.08	794	5.67	938	12.97	996	18.78	1018	1131	>52.7
8/1	503	0.42	1412	4.04	1500	4.42	702	0.97	1500	4.42	–	2006	>4.42
9/1	331	0.91	627	4.01	715	6.06	762	7.56	801	8.22	886	965	>27.6
9/2	546	0.67	1241	3.95	1389	5.46	1463	6.88	1500	7.54	1625	1739	>28.4
10/1	307	0.74	461	3.93	502	5.08	493	4.57	500	4.72	534	612	>60.8
10/2	420	0.57	950	3.99	1044	5.13	1062	5.41	1102	6.14	–	1284	>17.9
10/3	828	1.21	1230	4.09	1322	5.86	1491	10.09	1505	11.34	1519	1622	>75.1
11/1	1323	0.78	2406	4.66	2490	5.37	2641	6.96	2670	7.83	2832	3060	>45.6
11/2	1784	1.01	2585	4.42	2659	4.98	2937	7.51	2996	8.15	3150	3396	>43.9
11/3	1431	0.49	3802	4.81	3910	5.13	4428	8.11	4513	8.73	–	5092	>18.4
12/1	1240	1.89	2050	4.18	2362	6.33	2415	7.36	2396	6.72	2538	2918	>44.1

Table C Continued

Case No.	Interpreted uplift resistance, T[a] (kN), and the displacement, s[b, c] (mm)												
	T_{L1}	s_{L1}	T_{DA}	s_{DA}	T_{ST}	s_{ST}	T_{TI}	s_{TI}	T_{L2}	s_{L2}	$T_{T\&P}$	T_{CHIN}	s_{CHIN}
12/2	657	1.36	1390	4.03	2063	6.62	2110	7.65	2100	6.89	2272	2645	>38.6
12/3	615	2.27	1042	4.07	1539	9.98	1484	5.80	1500	6.08	1670	1999	>41.1
13/1	102	0.30	274	4.03	269	3.85	273	4.28	278	9.17	284	303	68.70
13/2	467	1.80	937	5.28	943	5.36	1075	7.90	1088	9.98	1099	1191	74.06
13/3	1256	1.40	1875	4.25	2037	5.91	2448	14.70	2530	19.20	2540	2826	73.78
13/4	332	1.37	522	3.98	581	5.72	769	19.40	853	35.80	798	943	70.24
13/5	1166	0.51	1580	4.19	1638	4.83	2068	14.20	2332	25.40	2321	2738	72.65
13/6	987	1.41	1238	4.33	1319	5.81	1499	17.80	1700	34.20	1587	2060	96.57
13/7	816	1.07	1361	4.15	1403	5.19	1526	14.00	1616	21.40	1624	1976	95.29
13/8	626	1.01	922	4.12	943	4.57	1108	15.80	1205	26.42	1193	1364	70.00
13/9	1304	0.91	2263	4.19	2422	5.50	2864	14.90	3524	50.15	3067	3765	82.84
13/10	1086	1.13	1733	4.85	1814	5.54	2355	15.26	2450	17.77	2550	3521	96.46
13/11	1330	1.41	2114	4.23	2640	7.17	3090	11.16	3631	19.71	3815	5664	75.87
14/1	365	1.41	532	4.17	592	6.09	755	16.01	803	21.87	811	935	62.93
14/2	809	1.82	1065	4.36	1144	6.12	1366	17.87	1510	33.19	1436	1639	53.85
14/3	1077	0.58	1621	4.69	1643	6.00	1925	17.66	2227	43.30	2340	2389	64.46
15/1	616	0.45	1033	4.07	1071	5.05	1199	13.42	1250	18.76	1278	1412	69.26
16/1	237	0.54	426	3.81	437	4.78	443	5.99	450	7.29	470	490	>32.7
16/2	854	1.85	1131	3.82	1247	6.39	1288	8.03	1326	10.10	1382	1526	>39.8
16/3	1516	1.64	2173	3.95	2568	6.87	2788	10.19	2875	12.10	2985	3436	>38.4
16/4	754	0.99	1667	4.09	1989	6.19	2235	11.65	2349	14.80	2423	2725	>37.6
16/5	2097	0.87	3610	4.03	3965	5.85	5378	17.64	6251	29.80	5930	6856	>42.5
16/6	1088	2.76	1304	4.11	1630	7.96	2021	17.37	2203	24.10	2210	2626	>44.4
16/7	2362	0.95	4593	4.41	5038	5.63	6233	10.64	7428	19.75	7789	8962	>32.1
16/8	1081	1.03	2101	4.32	2382	6.07	3425	19.07	3667	25.40	3659	4141	>48.1
16/9	2306	0.75	4554	4.79	4798	5.59	5850	11.24	7286	22.06	7467	8794	>32.5
17/1	154	1.71	218	3.78	294	7.08	346	12.81	361	14.70	371	424	>39.3
17/2	406	0.89	881	3.89	946	5.28	1043	11.37	1097	17.30	–	1247	>46.5
17/3	2848	1.34	3340	3.93	3508	5.75	3591	7.67	3659	11.00	3780	4092	>39.7
17/4	1547	4.63	1357	4.03	2129	10.05	2255	14.18	2349	17.70	2391	3250	>42.8
17/5	2097	2.77	4077	4.17	3111	2.54	5378	7.22	6251	14.46	–	6856	>14.81
17/6	1415	4.23	1374	4.18	2407	11.45	2678	16.21	2768	19.30	2814	3518	>44.8
17/7	2362	0.65	4794	3.82	5038	3.03	6233	3.60	7428	5.38	–	8962	>5.58
17/8	1140	3.78	1159	4.18	2977	15.59	3264	19.91	3395	22.42	3415	4939	>45.1
17/9	2270	4.03	4053	4.61	4717	13.27	5103	7.83	7286	13.70	–	8794	>45.14
18/1	327	2.41	408	3.88	524	7.86	555	10.30	576	12.40	603	735	>34.5
18/2	1088	3.17	1179	3.87	1633	8.64	1650	8.75	1668	11.00	1724	2000	>41.9
18/3	2844	2.61	3478	4.11	4074	7.34	4471	11.19	4524	12.60	4578	5214	>49.5

Table C Continued

Case No.	Interpreted uplift resistance, T[a] (kN), and the displacement, s[b, c] (mm)												
	T_{L1}	s_{L1}	T_{DA}	s_{DA}	T_{ST}	s_{ST}	T_{TI}	s_{TI}	T_{L2}	s_{L2}	$T_{T\&P}$	T_{CHIN}	s_{CHIN}
18/4	2306	4.73	2075	4.16	3120	10.19	3104	9.61	3246	14.80	3334	4292	>30.2
18/5	2750	1.30	4366	4.13	5105	6.29	7937	18.87	8273	22.56	8307	10400	>36.6
18/6	2325	3.38	2541	4.43	2986	8.05	3136	10.79	3211	13.10	3296	4219	>38.7
18/7	3144	2.31	4194	4.44	6692	8.56	8278	17.47	8150	20.17	8587	9480	>37.5
18/8	2330	2.66	2995	4.78	3400	7.39	3930	15.88	4260	24.13	4272	4840	>38.6
18/9	3093	1.47	5225	5.14	6673	6.01	5387	3.77	8571	9.80	–	9800	>10.09
19/1	529	1.25	604	4.04	608	5.16	599	2.28	604	3.90	604	694	>35.3
19/2	513	2.28	792	3.96	1163	8.71	1132	7.43	1155	8.50	–	1830	>16.4
19/3	658	1.04	1841	4.23	1961	6.85	1931	5.23	1955	5.70	–	2501	>12.4
19/4	1072	1.39	1555	3.97	1823	6.26	1830	6.57	1900	7.79	–	2153	>20.1
19/5	3182	6.10	2273	4.27	4555	12.43	4378	10.38	4522	11.50	–	5750	>19.9
19/6	1778	1.90	3064	4.15	3315	7.23	3278	5.24	3288	5.70	3536	3874	>29.5
19/7	1855	1.40	3524	4.27	4410	7.21	4234	6.48	4592	8.50	–	6397	>22.1
20/1	227	1.60	520	3.85	629	6.40	670	7.82	724	8.90	796	885	>37.1
20/2	765	0.60	985	4.25	1097	5.03	1706	8.46	2129	10.30	1691	2502	>36.8
21/1	476	0.90	649	3.83	728	5.80	754	7.72	761	13.80	784	833	>36.2
21/2	342	0.70	719	3.88	780	5.30	869	14.72	904	17.60	958	1037	>44.2
21/3	928	2.40	1920	4.01	2187	6.95	2377	13.23	2637	19.50	2893	3295	>36.6
21/4	894	1.00	1256	3.94	1390	5.09	1848	17.81	1895	30.50	1914	2025	>57.6
21/5	1237	1.49	2256	4.01	2550	6.99	3038	12.62	3322	19.40	3396	4103	>36.7
21/6	1365	1.10	2090	4.36	2188	6.55	3050	18.27	3355	22.30	3237	3714	>41.2
21/7	2163	1.00	3569	4.47	3990	6.48	5922	8.68	6561	12.40	6007	7179	>25.4
21/8	1424	1.70	2487	4.64	2897	6.03	4058	25.80	4228	52.20	4240	4779	>86.8
21/9	3834	2.66	5821	5.08	8599	9.97	8075	8.24	8490	9.22	–	8718	>12.14
22/1	826	0.60	1618	4.18	1657	4.93	1798	7.58	2017	11.70	2560	2509	>31.8

[a] Interpreted resistances for the various methods: T_{DA}, Davisson method; T_{ST}, Slope tangent method; T_{TI}, Tangent intersection method; T_{L1}, L_1 method; T_{L2}, L_2 method; $T_{T\&P}$, Terzaghi and Peck method; and T_{CHIN}, Chin method.

[b] Displacements for the various methods: s_{DA}, Davisson method; s_{ST}, Slope tangent method; s_{TI}, Tangent intersection method; s_{L1}, L_1 method; s_{L2}, L_2 method; $s_{T\&P}$, Terzaghi and Peck method; and s_{CHIN}, Chin method.

[c] by definition, $s_{T\&P}$ = 25.4 mm, not included in the Appendix.

[d] The symbol (–) expresses that the interpreted $T_{T\&P}$ values are not available.

[e] The symbol (>) expresses that the interpreted displacements are greater than the measured data.

Appendix D

Table D Summary of predicted ultimate uplift resistance, model factor, and hyperbolic curve fitting parameters *a* and *b* for belled piers in axial uplift.

Case No.	T_{up} (kN)	M_T	*a* (mm)	*b*	Case No.	T_{up} (kN)	M_T	*a* (mm)	*b*
1/1	2238	1.153	0.808	0.883	2/1	1707	1.341	0.222	0.939
1/2	2244	1.074	0.316	0.918	2/2	1713	1.177	0.074	1.240
1/3	2250	1.138	0.390	0.969	3/1	1156	1.176	3.976	0.748
3/2	776	1.000	0.894	0.948	13/7	1644	0.983	0.990	0.890
3/3	760	1.218	2.970	0.695	13/8	999	1.206	0.960	0.960
3/4	949	0.955	1.541	0.857	13/9	2770	1.272	1.900	1.010
3/5	1022	0.671	2.966	0.781	13/10	3024	0.810	2.977	0.759
3/6	1364	0.900	1.098	1.037	13/11	5069	0.716	4.788	0.673
4/1	1033	1.054	1.433	0.789	14/1	1277	0.629	2.102	0.907
4/2	1037	1.040	6.815	0.795	14/2	1988	0.759	1.753	0.965
4/3	1065	1.320	0.689	0.972	14/3	3554	0.627	1.008	1.045
4/4	1070	1.030	0.726	1.023	15/1	4235	0.295	0.671	0.954
5/1	1021	0.726	2.397	0.846	16/1	363	1.239	0.680	0.880
5/2	1025	0.722	4.737	0.679	16/2	1185	1.119	1.620	0.830
5/3	1105	0.681	1.556	0.817	16/3	2837	1.013	2.240	0.820
5/4	1110	0.656	2.299	0.821	16/4	1918	1.225	2.470	0.840
6/1	916	0.537	0.159	0.811	16/5	5092	1.228	2.590	0.960
6/2	2195	0.688	0.644	0.878	16/6	1992	1.106	3.650	0.850
6/3	4234	0.336	4.577	0.705	16/7	7337	1.012	2.980	0.860
7/1	1115	0.992	1.757	0.906	16/8	2393	1.533	3.360	0.910
7/2	1120	0.893	1.258	0.932	16/9	7702	0.946	2.880	0.860
7/3	1124	0.893	1.402	0.912	17/1	483	0.747	3.270	0.810
7/4	1128	0.883	1.452	0.928	17/2	1516	0.724	1.680	0.870
8/1	1103	1.360	1.339	0.734	17/3	3545	1.032	1.420	0.860
9/1	1072	0.747	1.638	0.833	17/4	2421	0.970	4.960	0.730
9/2	1711	0.877	1.356	0.855	17/5	6307	0.991	4.870	0.690
10/1	1089	0.459	0.903	0.826	17/6	2540	1.090	5.380	0.750
10/2	1525	0.723	1.076	0.860	17/7	9058	0.820	2.500	0.390
10/3	1976	0.762	1.004	0.927	17/8	3030	1.120	9.530	0.570
11/1	1650	1.618	0.880	0.898	17/9	9562	0.762	9.040	0.350
11/2	2412	1.242	1.056	0.884	18/1	461	1.250	2.840	0.780
11/3	3370	1.339	1.236	0.897	18/2	1488	1.121	2.900	0.770
12/1	1576	1.521	2.249	0.768	18/3	3543	1.277	2.600	0.800
12/2	1148	1.830	2.817	0.754	18/4	2448	1.326	3.850	0.750
12/3	803	1.869	2.868	0.723	18/5	6473	1.278	3.380	0.790
13/1	302	0.921	0.820	0.900	18/6	2552	1.258	3.210	0.750
13/2	894	1.218	1.470	0.910	18/7	9455	0.862	4.400	0.670

Table D Continued

Case No.	T_{up} (kN)	M_T	a (mm)	b	Case No.	T_{up} (kN)	M_T	a (mm)	b
13/3	2079	1.217	1.780	0.900	18/8	3105	1.372	9.970	0.300
13/4	752	1.134	2.280	0.950	18/9	9961	0.860	4.010	0.690
13/5	1876	1.243	0.440	1.060	19/1	665	0.909	1.040	0.800
13/6	1391	1.222	1.150	0.930	19/2	972	1.189	3.250	0.640
19/3	1577	1.240	1.860	0.730	21/3	2995	0.880	2.090	0.820
19/4	1599	1.188	1.420	0.850	21/4	1980	0.957	0.790	1.060
19/5	3458	1.308	5.530	0.580	21/5	4140	0.802	2.980	0.840
19/6	3028	1.086	1.710	0.790	21/6	4076	0.823	1.890	0.990
19/7	4135	1.111	2.470	0.730	21/7	5552	1.182	3.550	0.950
20/1	1112	0.651	2.240	0.810	21/8	3843	1.100	3.320	0.890
20/2	3073	0.693	5.460	0.930	21/9	10970	0.774	4.350	0.620
21/1	589	1.292	1.350	0.860	22/1	3980	0.507	0.820	0.790
21/2	1291	0.700	1.250	0.890					